

EXPERIMENTAL AND ANALYTICAL ASSESSMENTS OF MULTIPLE-SITE CRACKING IN AIRCRAFT FUSELAGE STRUCTURE

Dr. John G. Bakuckas, Jr.[†], Mr. Edem Akpan[‡], Mr. Peilin Zhang[‡], Dr. Catherine A. Bigelow[†],
Dr. Paul W. Tan[†], Professor Jonathan Awerbuch^{*}, Professor Alan Lau^{*}, and Professor T. M. Tan^{*}

An experimental and analytical assessment of multiple-site cracking in fuselage structure has been initiated in this study. The Full-Scale Aircraft Structural Test Evaluation and Research (FASTER) facility was developed to test full-scale fuselage panel specimens under conditions representative of those seen by an aircraft in actual operation. A global-local hierarchical (GLH) approach using the finite element method (FEM) was used to determine the strain distributions and the fracture parameters governing crack initiation and growth in fuselage structure. Comparisons with strain gage data verified the finite element analyses developed. A description of the FASTER facility and representative experimental and analytical results from a test panel containing a single crack in the middle of a skin bay are presented. Results shown include strain distributions, crack growth, and crack bulging characteristics. These findings provide the methodology for future testing and analysis.

INTRODUCTION

Since the 1988 Aloha Airlines accident in which a large portion of the fuselage crown of a Boeing 737 tore apart due to the link-up of small cracks emanating from rivet holes in the lap joint, much effort has been placed on developing methodologies to predict the reduction in residual strength of aircraft fuselage structure due to various multiple-site cracking scenarios. Research efforts sponsored by the Federal Aviation Administration (FAA), National Aeronautics and Space Administration (NASA), and the Department of Defense (DoD) include the development of various analytical tools that address this complex problem at several levels. Both rigorous numerical methods and simplified engineering approaches have been developed to predict crack initiation, growth and link-up, and residual strength [1-9]. In general, the development of each tool has been focused on analyzing different aspects of the process, such as crack initiation, crack growth, crack link-up, or residual strength of the fuselage structure. Combined, these tools can predict the entire process and can be used in the current fleet of

[†] AAR-431, William J. Hughes Technical Center, Atlantic City International Airport, NJ 08405, USA

[‡] Graduate Student, Department of Mechanical Engineering and Mechanics, Drexel University, Philadelphia, PA 19104, USA

^{*} Faculty, Department of Mechanical Engineering and Mechanics, Drexel University, Philadelphia, PA 19104, USA

aircraft to predict the effect of multiple-site cracks on the residual strength or in future aircraft designs to prevent the occurrence of multiple-site cracking within the design life of the structure.

As part of the FAA research program, a two-prong research effort is being conducted at the FAA William J. Hughes Technical Center to assess the effects of multiple-site cracking on the residual strength of fuselage structures. One focus of the research effort is on developing computational methods including the finite element analysis method to determine fracture parameters governing the onset and growth of cracks and the residual strength of fuselage structure with multiple-site cracks. These methods will be used to predict strain distributions, crack growth and bulging, and residual strength.

The second focus is on conducting tests to understand the damage mechanics and guide the model development. A unique, state-of-the-art Full-Scale Aircraft Structural Test Evaluation and Research (FASTER) facility was developed to apply realistic flight load conditions to large curved sections of fuselage structure. Both quasi-static and spectrum loadings can be applied including differential pressure, longitudinal load, hoop load in the skin and frames, and shear load. The test data will be used to validate analytical methodologies developed by the FAA and NASA [9]. The FASTER facility is located at and operated by the FAA William J. Hughes Technical Center.

This paper reports on testing and analysis that was done with the FASTER test fixture to establish the methodologies for testing and analyzing fuselage structure with multiple-site cracking scenarios. A strain survey was conducted under quasi-static loading conditions on a test panel to verify proper load transfer from the load application points to the panel. Crack growth and crack bulging of a single crack located in the middle of a skin bay under fatigue loading conditions were measured. In the following sections a brief description of the FASTER test fixture along with representative analytical and experimental results are presented. Results include comparisons of strain distributions, damage growth process, and crack growth characteristics. These findings provide the experimental and analytical procedures for testing curved panels containing multiple-site cracking scenarios.

DESCRIPTION OF FACILITY

The FASTER test fixture, shown in Figure 1, combines mechanical, fluid, and electronic components to apply internal pressure, longitudinal, hoop, frame, and shear loads to a curved panel. As shown in the exploded view in Figure 1, the fixture consists of a base structure, a hoop load assembly, a longitudinal load assembly, a pressure box, a frame load assembly, and a shear fixture assembly. The FASTER facility also includes a computerized instrument control and data acquisition system and a remote control crack monitoring (RCCM) system not shown in Figure 1. A full description of the FASTER facility is provided in reference 10. For completeness, a brief description is provided here in.

The test panel is attached to the pressure box using an air-tight elastomeric seal. Internal pressure is applied to the panel using air or water. Mechanical loading mechanisms consisting of water actuators, load cells, and whiffle tree assemblies with a lever arm configuration are used to apply the hoop and longitudinal loads around the perimeter of the test panel. Hoop forces are

applied by individual loading linkages using a two-tier, coaxial whiffle tree assembly, which generates four equal forces from each lever arm. Seven lever arms or load points are used on each side of the specimen for a total of 28 attachment points. Longitudinal forces are applied using similar loading devices on each end of the panel, consisting of 4 load points and 16 attachment points on each end. Hoop loads are applied at each end of each frame using a similar loading mechanism.

An innovative shear load application system was developed that uses two load distribution points in the longitudinal direction, one on either edge of the specimen. The force is applied as a couple and is reacted by a couple in the hoop direction. A unique feature of the shear loading system is the elastomeric coupling between the loading mechanisms and the test specimen. The elastomer, which has a low shear modulus, creates a close approximation to uniform shear distribution in both the applied and reacted couples.

All forces are generated using water or air. The external loads are generated by applying water pressure to water actuators, which are controlled by pressure-activated dome valves. The dome valves are automatically controlled by electro-pneumatic (E/P) control valves. The E/P valves are driven by a computer control system in a closed-loop configuration using the feedback from the load cells. The operator can control the loads, speed, and type of test. Data from strain transducers, load transducers, pressure transducers, etc., are displayed on color monitors in real time and stored for subsequent analysis.

Acceptance testing was conducted to verify that the FASTER test fixture met the specified design and operational requirements. The load assemblies were loaded to the full-scale levels to demonstrate that the fixture could sustain the appropriate design limits. Both quasi-static and fatigue loadings were applied using water and air as the panel pressurization media. Results of the acceptance test are reported in reference 10.

A Remote Controlled Crack Monitoring (RCCM) system was developed to track and record crack initiation and propagation during a test. The RCCM system is a stand-alone, computer-based video data acquisition system capable of monitoring the entire panel test surface at several levels of magnification with a field of view ranging from 0.05" to 14". Two black and white RS-170 format analog cameras are mounted to a remote controlled, high-precision x-y-z translation stage which provides real-time crack length measurement capabilities with a 0.0001" resolution.

A method to measure out-of-plane displacements was developed to determine the shape and extent of crack bulging. An array of linear variable differential translation (LVDT) displacement transducers oriented normal to the panel surface were used to measure the out-of-plane displacements at points on one side of the crack.

EXPERIMENTAL PROCEDURES

A series of tests were conducted using the FASTER facility. Quasi-static loading was applied to measure strain and crack bulging; fatigue loading was applied to measure crack extension. Three tests were conducted using quasi-static loading to measure strains in the panel. The fourth test

was a fatigue test in which crack growth was measured. In the fifth and final test, also using quasi-static loading, crack bulging was measured.

Test Matrix

The test matrix is shown in Table 1. For Test Cases 1–3, the strain was measured under quasi-static loading. For Test Case 1, pressure and hoop load in the skin and frames were applied; for Test Case 2, only longitudinal load in the skin was applied; and for Test Case 3, pressure, hoop load in the skin and frames, and longitudinal load were applied. The loads used in Test Case 3 were chosen to simulate a pressurization loading on a cylindrical fuselage structure. Test Cases 1-3 were repeated 4 times, twice using air and twice using water to pressurize the panel to evaluate any effects of the different pressurization media and to determine the repeatability of measurements. The load was applied in five equal increments up to the maximum values shown in the Table 1. At each load increment, the strain in the panel was recorded.

For Test Case 4, a constant-amplitude fatigue load was applied at a frequency of 0.125 Hz with an R-ratio (minimum to maximum load ratio) of 0.1 with the maximum load values shown in the Table 1. The maximum loads in Test Cases 3 and 4 were identical, again representing a cylindrical pressurization loading. Crack initiation and extension were measured in real time using the RCCM system.

For Test Case 5, the same loading condition as in Test Case 3 was used and the crack bulging profile was measured under quasi-static loading conditions. An array of LVDT displacement transducers oriented normal to the panel surface were used to measure the out-of-plane displacements at points along one side of the crack.

Table 1. Test Matrix

Test Case	Test Type	Loading Rate (Hz)	Maximum Load			
			Pressure (psi)	Hoop (lb./in)	Frame (lb./in)	Long. (lb./in)
1	Strain Survey	0.00833	5	283.8	46.2	0
2	Strain Survey	0.00833	0	0	0	504
3	Strain Survey	0.00833	5	283.8	46.2	165
4	Crack Growth	0.125	5	283.8	46.2	165
5	Crack Bulge	0.00833	5	283.8	46.2	165

Test Panel Configuration

Figure 2 shows a drawing of the test panel which had a radius of 66" and a skin thickness of 0.05". The panel was cut from the fuselage of a narrow-body aircraft and contains six frames (labeled F1 through F6) and seven stringers (labeled L3 through L9). The panel contains a longitudinal lap splice located along stringer L7. Reinforcing doublers were added around the perimeter of the panel to attach to the whiffle tree assemblies. Doublers were also added to the frame ends to attach to the frame loaders.

The panel was instrumented with 36 strain gages on the fuselage skin, frames, and stringers as indicated in Figure 2. The bars indicate the direction of the strain measured. A number in a solid line circle indicates a strain gage that is on the inner surface; a number in a dashed line circle indicates a strain gage on the outer surface of the panel. Strain gages 28 through 36 were three-legged rosette strain gages where A, B, and C designate the longitudinal, 45°, and hoop directions, respectively. All other strain gages were uniaxial.

Using a jeweler's saw, a crack-like slit of half-length, $a_o = 2.33$ " and width = 0.06", was cut in the skin in the middle bay between stringers L4 and L5 and frames F4 and F5. To keep the panel water and air tight, a 0.05" thick rubber seal was bonded on the inner surface of the panel over the crack. Crack propagation gages were installed at each crack tip to monitor crack extension.

ANALYSIS

Geometric nonlinear finite element analyses were conducted using the commercial finite element code ABAQUS 5.8 [11]. Two analyses were conducted: first to model the pressure loading of a complete fuselage section, and the second to model the test panel to predict displacements and strains in the panel under the loading applied by the FASTER fixture. Results from the two analyses were compared to determine how well the analysis of the FASTER fixture matched an analysis of a complete fuselage section. To predict the crack growth behavior in the test panel, the stress-intensity factor (SIF) solutions governing crack extension were calculated.

Description of Models

To analyze the pressurization of a complete fuselage section, due to symmetry it was necessary to model only a section of the cylinder; the model of a 45° cylindrical section, shown in Figure 3, was developed. In the analysis, the skin, the frames, the stringers, and the shear clips were explicitly modeled as shown in Figure 3. The skin was modeled using 8-noded shell elements and beam elements were used to model the frames, shear clips, and stringers. The model contains 7467 shell elements and 84 beam elements. Each frame and shear clip pair was modeled using a single beam with the combined cross-sectional properties of the frame and shear clip. Each stringer was modeled using a single beam with the cross-sectional properties of the stringers. The skin, stringer, frame, and shear clips were held together using nodal multipoint constraints. Symmetry boundary conditions were applied to two edges of the model; the displacement in the angular direction, u_θ , and the rotations about the radial axis, θ_r , and longitudinal axis, θ_z , were constrained to zero. On one end of the model, the longitudinal displacement, u_z , and the rotations about the radial axis, θ_r , and the angular axis, θ_θ , were constrained to zero. On the other end of the model, a traction in the longitudinal direction, $T_z = pR/2$, was applied where $p = 5$ psi is the internal pressure and $R = 66$ " is the cylinder radius. Internal pressure, p , was applied to the inside surface of the skin. A very refined mesh was used to model the crack vicinity in the center of a skin bay.

The finite element model of the test panel is shown in Figure 4. The finite element mesh of the test panel contains 25344 4-noded shell elements to model the skin, frames, shear clip, stringers, and intercostals; and 12 beam elements to model the radial reaction links. The cross section of the stringers, frames, shear clips, and intercostals were modeled using shell elements. The skin,

stringer, frame, and shear clips were connected using 1634 beam elements with a shear stiffness given by a variant of the equation developed by Swift [12]:

$$k_{shear} = \frac{E' d}{5 + 0.8 \left(\frac{d}{t_1} + \frac{d}{t_2} \right)} \quad (1)$$

where $E' = 10.5 \times 10^6$ psi is the effective modulus, $d = 0.1875$ " is the fastener diameter, and $t_1 = 0.05$ " and $t_2 = 0.05$ " are the thickness of the skin and substructure (shear clip or stringer), respectively.

The load conditions specified in Table 1 were simulated in the analysis. For the hoop, frame, and longitudinal loads, nodal point forces were applied at the load application points in the actual test as shown by the arrows in Figure 4. Internal pressure was applied to the inner surface of the skin.

Global-Local Hierarchical Approach

A global-local hierarchical (GLH) approach, based on the finite element method, was used to calculate the stress-intensity factors. The GLH approach was developed and verified in studies of crack bulging in pressurized curved panels [13] and cracks emanating from holes in three-dimensional solids [14,15]. The GLH approach is shown in Figure 5 where a geometric nonlinear shell analysis was used for the global model. The model used for the global level analysis is the same model described in the previous section used to analyze the test panel. The displacements defining the boundary of the local model were determined from the global model using the submodeling features available in ABAQUS 5.8. The three-dimensional local model consists of two layers of 20-noded brick elements totaling 3520 elements.

Fracture Parameters

The variation of the J-integral along the crack front was calculated at points a through e shown in Figure 5. Since the elements have the same thickness along the crack front, the average J-integral was calculated by treating the J-integral values as equivalent nodal forces having units of forces per unit length:

$$J_{avg} = \frac{J_a + 4J_b + 2J_c + 4J_d + J_e}{12} \quad (2)$$

For the current configuration and applied loading, the crack-tip deformation is primarily mode I. Assuming plane stress conditions, the mode I stress-intensity factor can be calculated as:

$$K_{curve} = \sqrt{J_{avg} E} \quad (3)$$

where $E = 10.5 \times 10^6$ psi is the modulus of elasticity for the skin of the test panel. The GLH approach was used to calculate the stress-intensity factor as a function of crack length for the test panel. The baseline crack growth rate data for thin sheet 2024-T3 aluminum (shown in

Figure 7.5.3.1.19 of reference 16) was used with the calculated stress-intensity factors to predict crack growth in the test panel.

In addition, the crack growth in the unstiffened shell structure was also calculated using an engineering approximation based on a bulging factor calculation. The bulging factor, β , is defined as the ratio of the stress-intensity factor of a curved panel to that of a flat panel:

$$\beta = \frac{K_{curve}}{K_{flat}} \quad (4)$$

The following approximation for the bulging factor in unstiffened curved panels was developed using a dimensional analysis with finite element data [12]:

$$\beta = 1 + 0.775 \sigma \sqrt{\pi a} \left(\frac{E}{\sigma} \right)^{1/3} \left(\frac{a}{R} \right)^{5/6} \quad (5)$$

Defining the reference stress, σ , using the hoop stress, the stress-intensity factor for the flat panel is:

$$K_{flat} = \frac{pR}{t} \sqrt{\pi a} \quad (6)$$

where p is the applied pressure, R is the panel radius, t is the skin thickness, and a is the half crack length. Using Equations 4 through 6, the expression for the curved-panel stress-intensity factor is then:

$$K_{curve} = \frac{pR}{t} \sqrt{\pi a} \left(1 + 0.775 \frac{pR}{t} \sqrt{\pi a} \left(\frac{E}{pR/t} \right)^{1/3} \left(\frac{a}{R} \right)^{5/6} \right) \quad (7)$$

Since stiffness effects of frames and stringers are not considered in the engineering approach, the results calculated using Equation 7 should be conservative. The engineering approach provides a quick, yet conservative, estimate of crack growth.

RESULTS AND DISCUSSION

Representative results of the strain gage survey, crack growth, and crack bulging are discussed in the subsequent sections.

Strain Distribution

The strain distribution in the panel was measured and predicted for each of the loading conditions listed in Table 1 at the strain gage locations shown in Figure 2.

Representative results from Test Case 1 are shown in Figure 6. The measured and predicted hoop strain at gage 31C in the center of the panel is plotted as a function of load step. As shown in the figure, the strains are nearly identical for all four runs. As expected, there were no differences in the results when air or water was used to pressurize the panel. Predictions from analyses shown by the curves in Figure 6 were in excellent agreement with the experimental data validating the finite element analysis. The predictions from analysis of the test panel shown by the solid line were similar to the predictions from the analyses of the cylindrical section shown by the dashed line. This indicates that the loading conditions used for the test panel model correctly simulate the pressurization of a full fuselage.

For Test Case 2, the measured and predicted longitudinal strain at gage 31A is plotted as a function of the load step in Figure 7. For Test Case 3, the measured and predicted hoop strain at gage 34C located in the skin by the lap splice region at stringer 7 is plotted as a function of the load step in Figure 8. As shown in these figures, the measurements from the test with water and with air were similar and excellent agreement was obtained between experimental data and the analysis of the test panel.

The measured and predicted longitudinal strain in the skin in the middle of the panel as a function of load for Test Case 2 is shown in Figure 9. The open symbols shown are the averages of each strain gage for the four tests. The solid symbols are the predictions from the test panel analysis and, again, excellent agreement was obtained between the experiments and the analysis. As shown, the distribution of strain through the middle of the panel is nearly equal at gages 31A and 35A. On either end of the panel at gages 28A and 36A in the outermost skin bays, the value of strain is higher near the boundary of the panel.

Similar trends were measured for the other strain distributions. In general, for the loadings used, a uniform strain distribution was obtained in the middle of the panel. Once away from the loading points on the edge of the panel by a minimum of one stringer or frame spacing, the panel boundary did not affect the strain distribution; this area is enclosed by the bold line on the insert in Figure 9.

Crack Growth

The stress-intensity factor range, which was calculated using the GLH approach, is plotted as a function of crack length for Test Case 4 in Figure 10. The dashed line is the stress-intensity factor range, determined using the engineering approach with Equation 7. The stiffness effects from frames and stringers were not included in Equation 7 resulting in higher values in the stress-intensity factor range compared with the GLH approach.

Figure 11 shows the fatigue crack growth under constant amplitude loading for Test Case 4 recorded at each crack tip using the RCCM system. The crack extension from the two crack tips is similar and colinear. This indicates a uniform load in the region of the crack.

The crack length, as a function of number of cycles, is shown in Figure 12 for Test Case 4. The circular and triangular symbols are the measured crack lengths at the left and right crack tips, respectively. The solid line is the prediction made using the engineering approach and Equation

7. The dashed line is the prediction made using the GLH approach and the test panel finite element model. As shown, good agreement with experiments was obtained using the GLH approach. As expected, the predictions were made using stress-intensity factor solutions from the engineering approach, which neglects the frame stiffness, were conservative. More accurate predictions were made with the GLH approach which accounts for the major structural details such as the frame cross section.

Crack Bulging Profile

The measured and predicted out-of-plane displacements along the length of the crack at a distance of 0.15" from the crack are shown in Figure 13 for Test Case 5. The half crack length was $a_f = 3.33$ " for the displacements shown. As expected, the out-of-plane displacement is highest at the centerline and the shape of the crack bulging profile is symmetric about the centerline. Results from analyses shown by the solid curve were in excellent agreement with the experimental data.

CONCLUDING REMARKS

An experimental and analytical research effort to assess the effects of multiple-site cracking on the residual strength of fuselage structures was conducted. A global-local hierarchical (GLH) analysis, based on the finite element method, was used to determine the strain distributions and the stress-intensity factors in a curved panel. The Full-Scale Aircraft Structural Test Evaluation and Research (FASTER) facility was used to apply realistic loading conditions to a curved panel representing a fuselage section. Both quasi-static and spectrum loadings were applied to the panel.

A curved panel containing a single crack in the middle of a skin bay was tested. Strains were measured under quasi-static loading conditions. In general, for the loadings used, a uniform strain distribution was obtained in the middle of the panel. Away from the edge of the panel by a minimum of one stringer or frame spacing, the effect of the panel boundary did not affect the strain distribution. The strain measurements were highly repeatable and were in excellent agreement with the finite element analysis. Predictions from the test panel model analysis were also in good agreement with those from the cylindrical section model analysis, indicating that the panel analysis simulated the pressurization of a full fuselage.

Symmetric, colinear crack extension from the crack tips under fatigue loading was measured using the Remote Controlled Crack Monitoring (RCCM) system. Good agreement was obtained between experimental data and predictions made using stress-intensity factors calculated by a finite element analysis of the test panel. The out-of-plane displacements measured under quasi-static loading conditions were symmetric, indicating the load transferred to the crack region was uniform. Predictions of crack bulging agreed with test data. This study provides the framework for further testing and analysis of curved-panel specimens representative of generic fuselage structures.

ACKNOWLEDGEMENTS

This research was supported in part by the FAA-Drexel Fellowship Program established by grant number 97-P-0052 from the Federal Aviation Administration William J. Hughes Technical Center.

REFERENCES

1. Newman, J. C., Jr., "A Crack-Closure Model for Predicting Fatigue Crack Growth Under Aircraft Spectrum Loading," *American Society for Testing and Materials Special Technical Publication 748*, 1981, pp. 53-84.
2. Newman, J. C., "Finite Element Analysis of Crack Growth Under Monotonic and Cyclic Loading," *American Society for Testing and Materials Special Technical Publication 637*, 1977, pp. 56-80.
3. Harris, C. E., Newman, J. C., Piascik, R. S., and Starnes, J. H., "Analytical Methodology for Predicting the Onset of Widespread Fatigue Damage in Fuselage Structure," *Proceedings of FAA-NASA Symposium on Continued Airworthiness of Aircraft Structures*, DOT/FAA/AR-97/2, July 1997, pp. 63-88.
4. Atluri, S. N. and Nishioka, T., *Engineering Fracture Mechanics*, Vol. 20, 1984, pp. 209-244.
5. Wang, L., Brust, F. W., and Atluri, S. N., "Predictions of Stable Growth of a Lead Crack and Multiple-Site Damage Using Elastic-Plastic Finite Element Alternating Method (EPFEAM)," *Proceedings of FAA-NASA Symposium on Continued Airworthiness of Aircraft Structures*, DOT/FAA/AR-97/2, July 1997, pp. 505-518.
6. Broek, D., "Effects of Multi-Site Damage on the Arrest Capability of Aircraft Fuselage Structures," *Fracture Research, Inc., USA*, TR 9302, 1993.
7. Swift, T., "Widespread Fatigue Damage Monitoring—Issues and Concerns," *Proceedings of 5th International Conference on Structural Airworthiness of New and Aging Aircraft*, Federal Republic of Germany, DGLR-Bericht 93-02, 1993, pp. 133-150.
8. Bakuckas, J. G., Nguyen, P. V., and Bigelow, C. A., "Bulging Factors for Predicting Residual Strength of Fuselage Panels," *Proceedings of the 19th Symposium of the International Committee on Aeronautical Fatigue, ICAF 97*, Edinburgh, United Kingdom, 1997, pp. 179-196.
9. Tan, P. W., Bigelow, C. A., and Bakuckas, J. G., Jr., "An Integrated Methodology for Assessing Widespread Fatigue Damage in Commercial Aircraft," *Seventh International Fatigue Conference, Fatigue '99*, Beijing, Peoples' Republic of China, June 8-12, 1999.
10. Bakuckas, J. G., Jr., Bigelow, C. A., and Tan, P. W., "The FAA Full-Scale Aircraft Structural Test Evaluation and Research (FASTER) Facility," *Proceedings from the International Workshop on Technical Elements for Aviation Safety*, Tokyo, Japan, 1999.

11. ABAQUS Version 5.8, Hibbitt, Karlsson, and Sorensen (HKS), 1080 Main Street, Pawtucket, RI 02860, USA, 1998.
12. Swift, T., "Development of the Fail-Safe Design Features of the DC-10," *American Society for Testing and Materials Special Technical Publication 486*, 1970, pp. 164-214.
13. Bakuckas, J. G., Jr., Nguyen, P. V., and Bigelow, C. A., "Bulging Factors for Predicting Residual Strength of Fuselage Panels," *Proceedings of the 19th Symposium of the International Committee on Aeronautical Fatigue, ICAF 97*, Edinburgh, United Kingdom, 1997, pp. 179-196.
14. Bakuckas, J. G., Jr., "Comparison of Boundary Correction Factor Solutions for Two Symmetric Cracks in a Straight-Shank Hole," DOT/FAA/AR-98/36, April 1999.
15. Rahman, A., Bakuckas, J. G. Jr., Bigelow, C. A., and Tan, P. W., "Boundary Correction Factors for Elliptical Surface Cracks Emanating from Countersunk Rivet Holes," *Proceedings from the 2nd NASA/FAA/DoD Conference on Aging Aircraft*, Williamsburg, VA, January 1999, pp. 598-609.
16. Skinn, D. A., Gallagher, J. P., Berens, A. P., Huber, P. D., and Smith, J., "Damage Tolerant Design Handbook," WL-TR-94-4054, Volume 3, Chapter 7, May 1994, pp. 7-214.

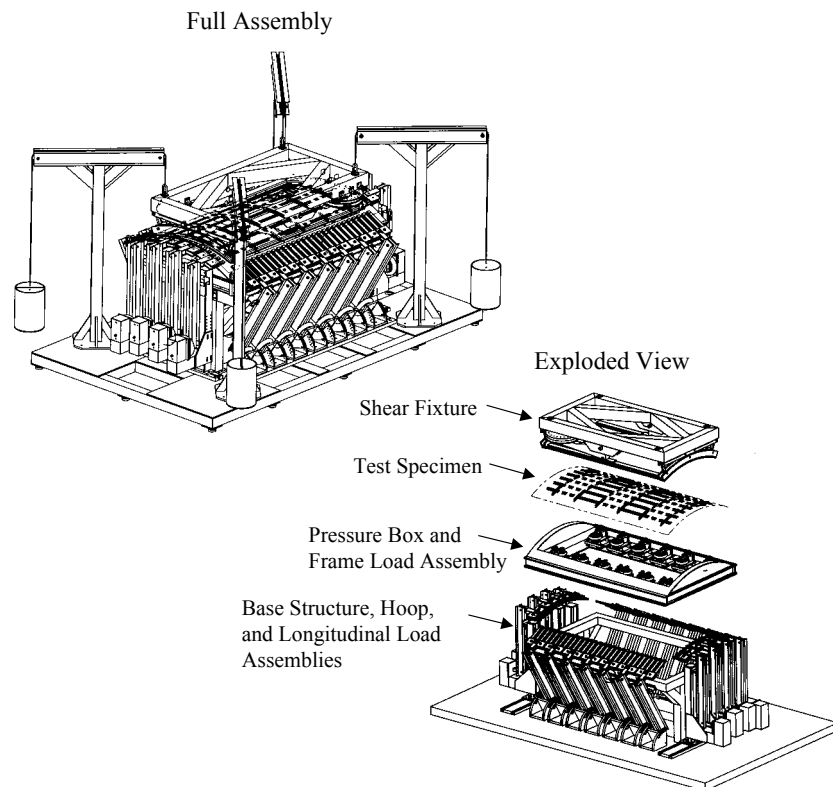


Figure 1. Full-Scale Aircraft Structural Test Evaluation and Research (FASTER) fixture.

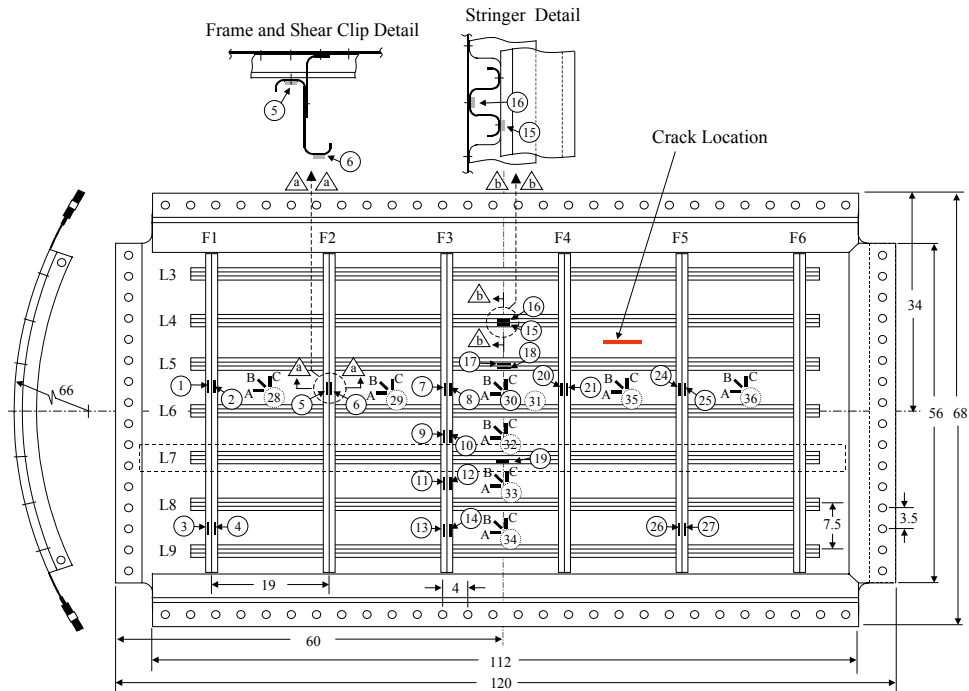


Figure 2. Schematic of test panel and location of strain gages. All units in inches.

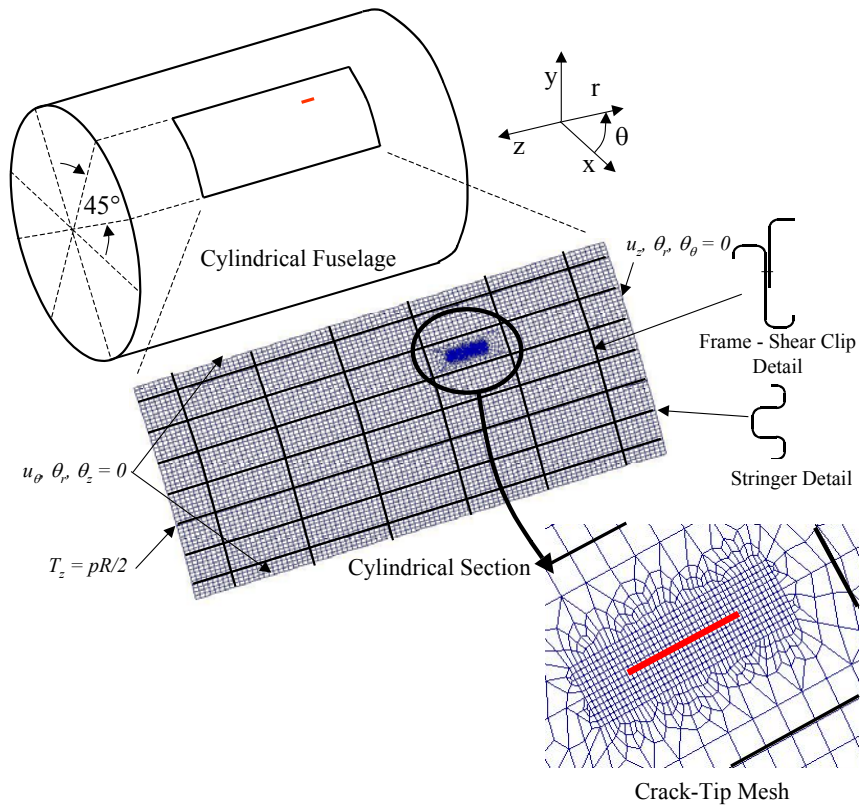


Figure 3. Finite element model of a cylindrical section taken from a complete section of the fuselage.

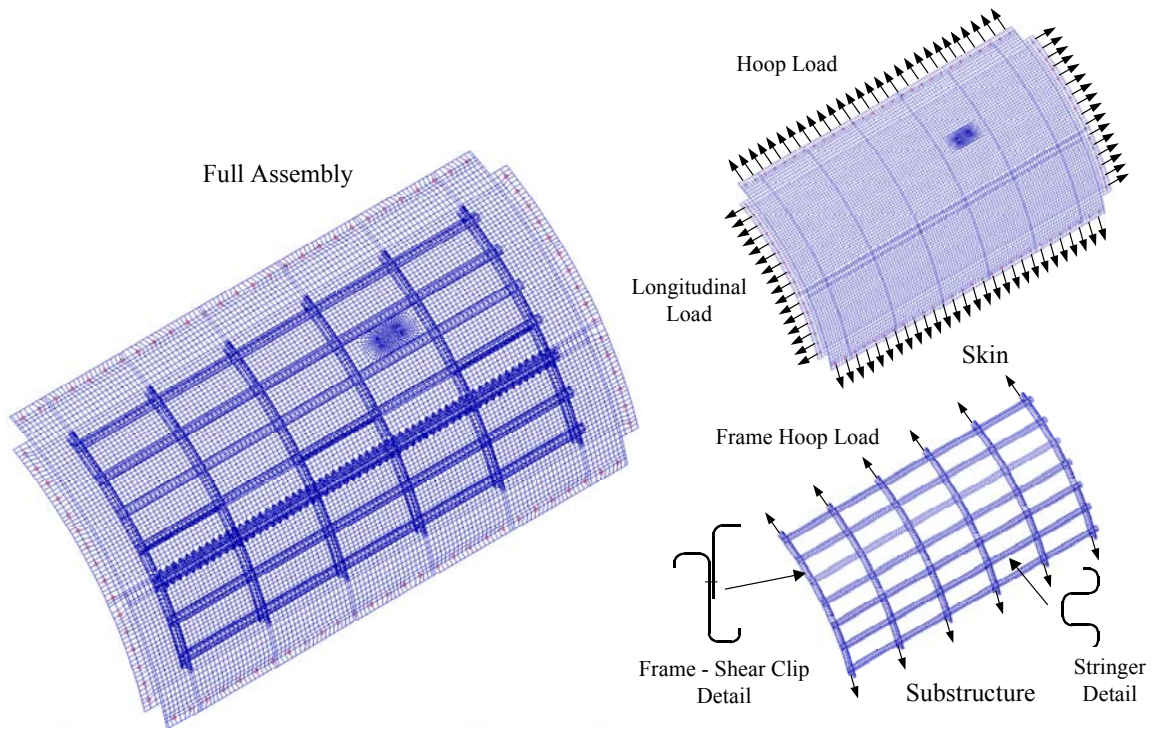


Figure 4. Global finite element model of test panel.

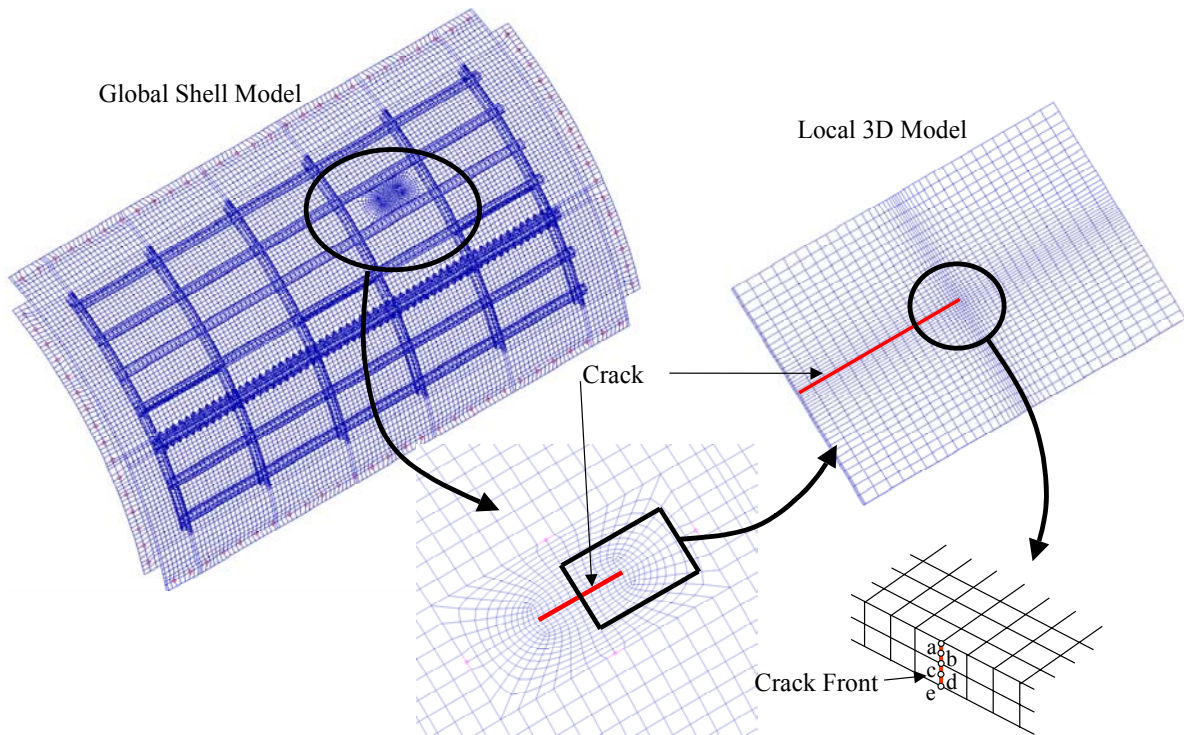


Figure 5. Global-local hierarchical (GLH) approach.

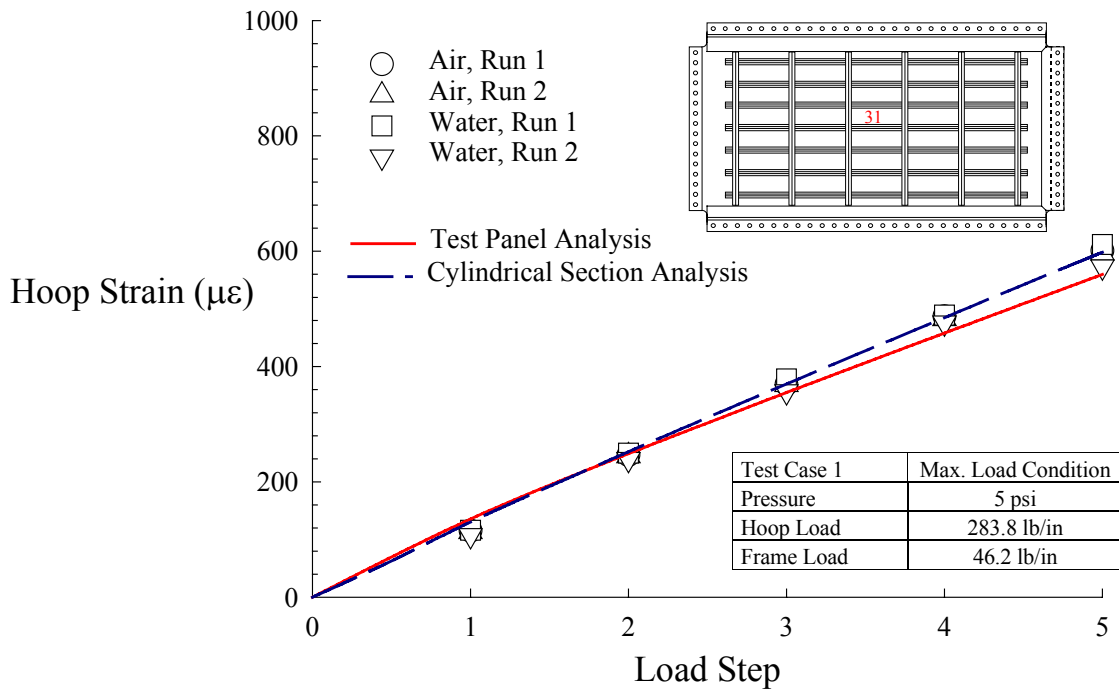


Figure 6. Hoop strain as a function of load step at strain gage 31C for Test Case 1.

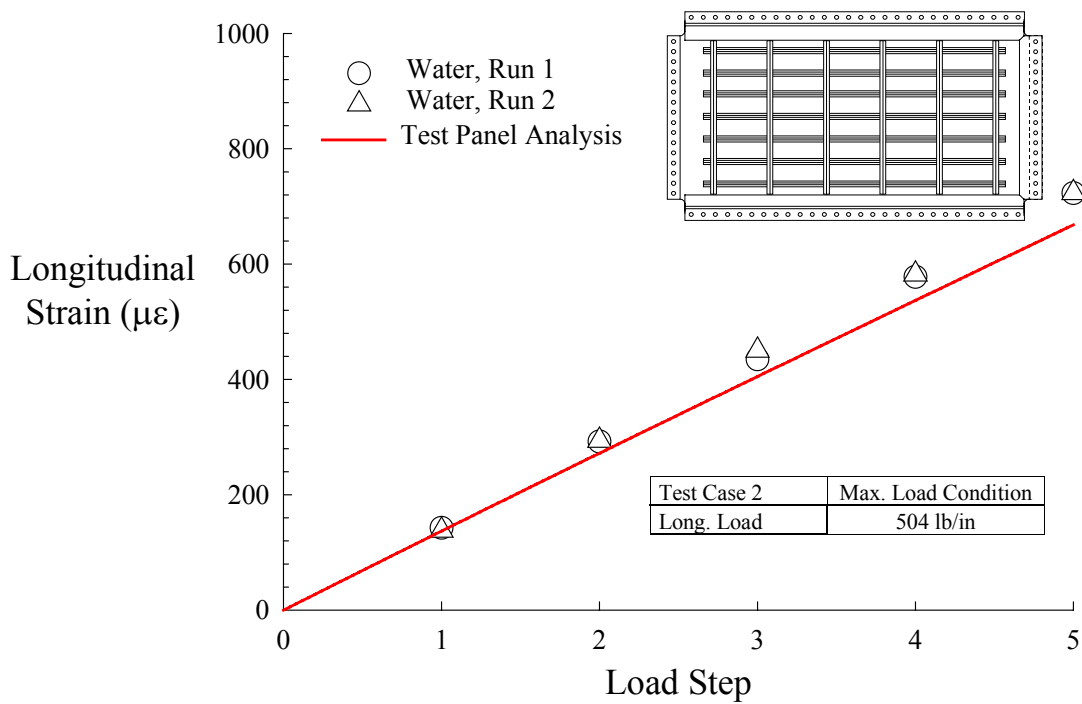


Figure 7. Longitudinal strain as a function of load step at strain gage 31A for Test Case 2.

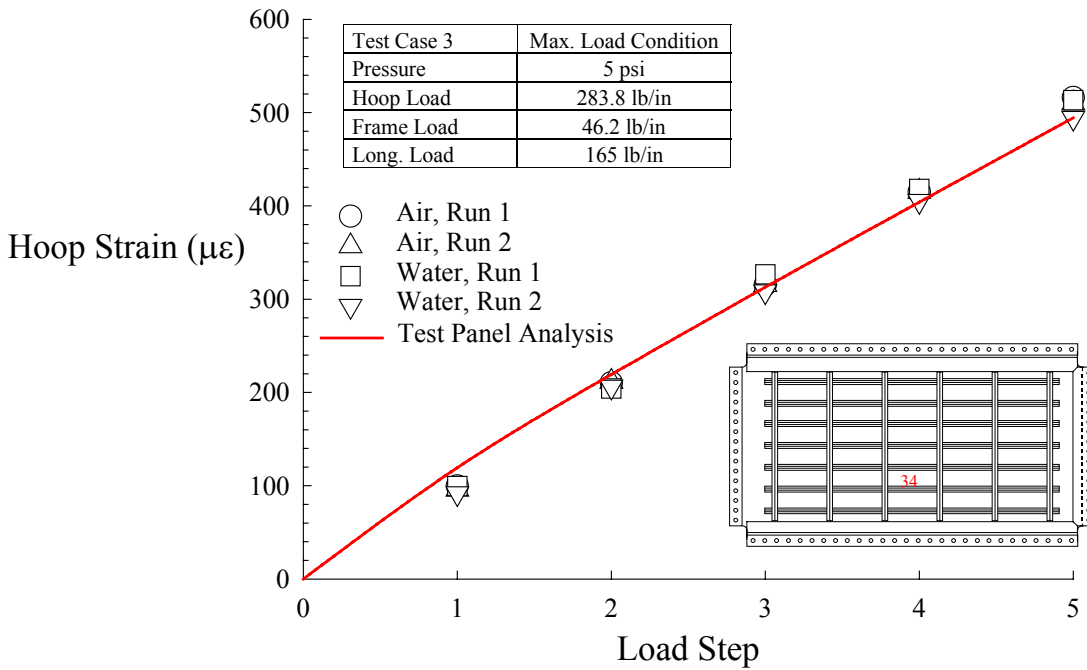


Figure 8. Hoop Strain as a function of load step at strain gage 34C for Test Case 3.

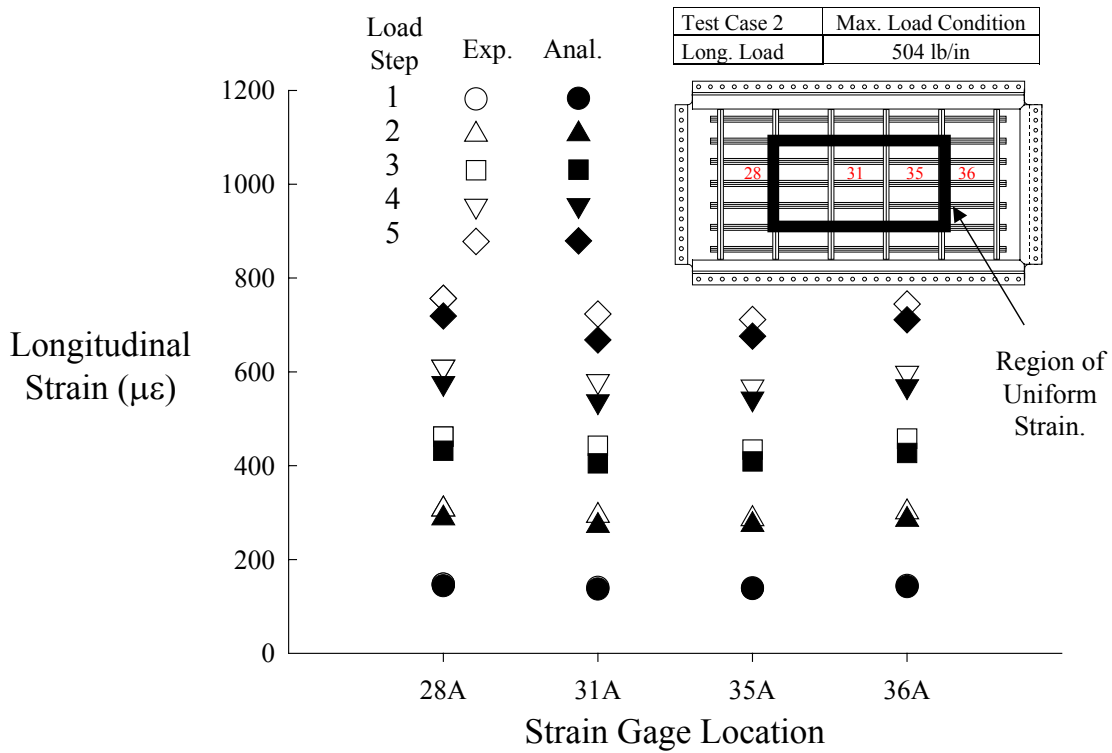


Figure 9. Longitudinal strain distribution in skin for Test Case 2. Results are averages from four tests.

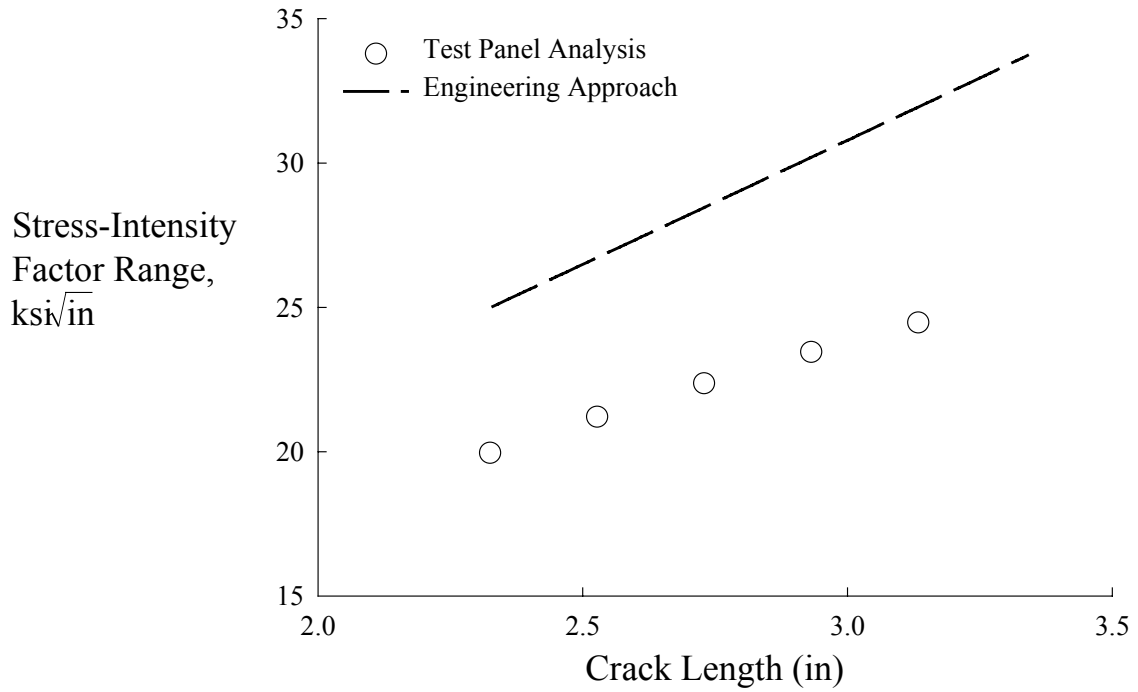


Figure 10. Stress-intensity factor range as a function of crack length.

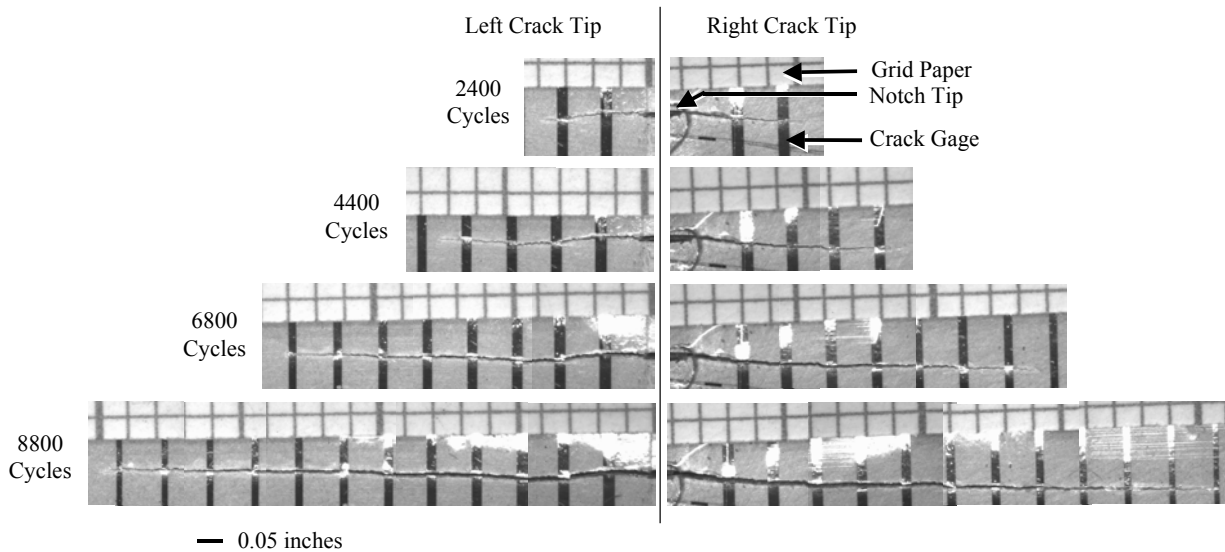


Figure 11. Images of crack extension at each crack tip using the Remote Control Crack Monitoring (RCCM) system.

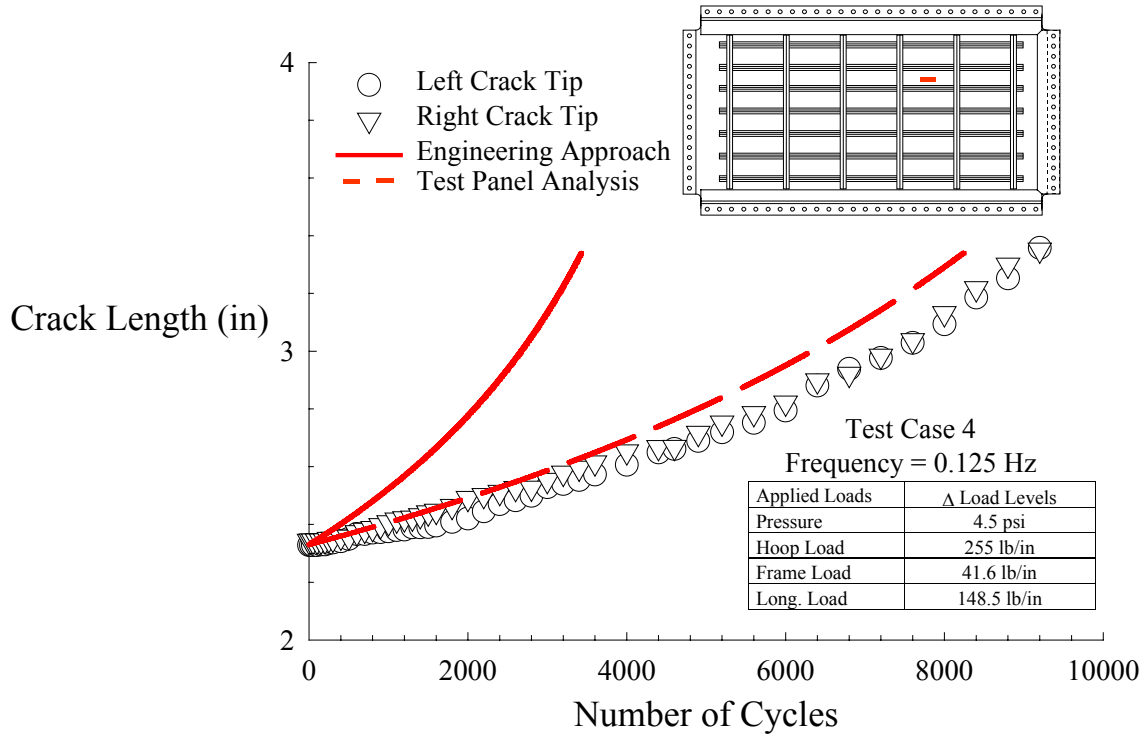


Figure 12. Crack length as a function of number of cycles.

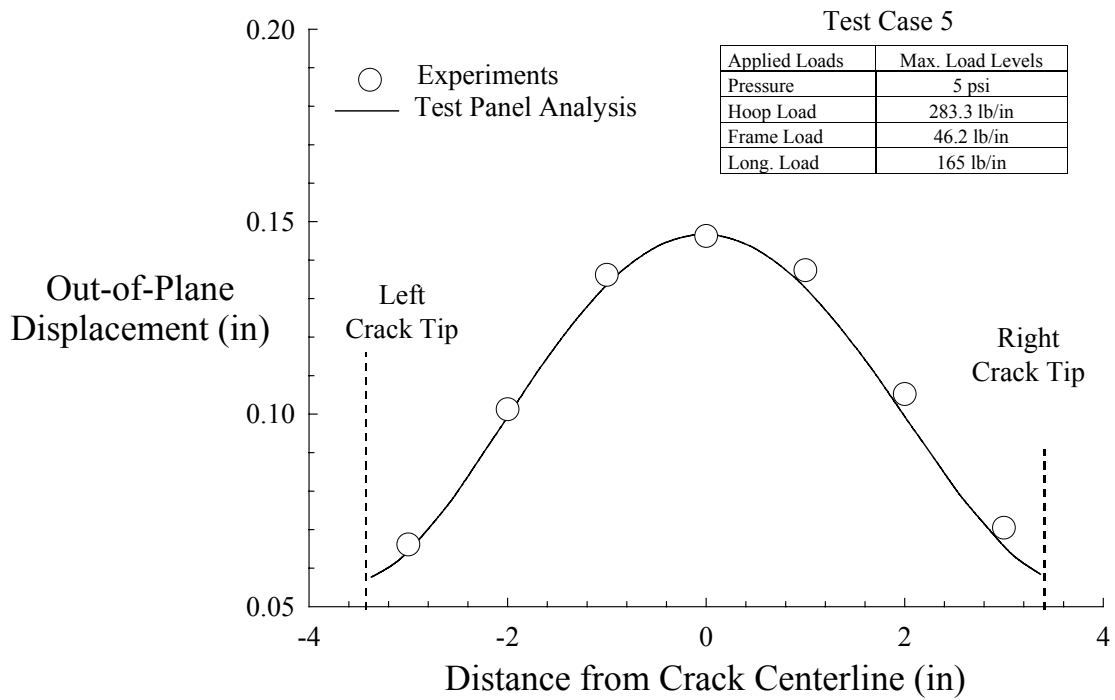


Figure 13. Crack bulging profile.